Thermohaline instability and the formation of glacial North Atlantic super polynyas at the onset of Dansgaard-Oeschger warming events

Guido Vettoretti[1] and W. Richard Peltier[1]

[1]Department of Physics, University of Toronto, Toronto, Ontario, Canada

Abstract Late Quaternary rapid warming events inferred on the basis of oxygen isotopic data from Greenland ice cores are the most prominent characteristic of millennial-scale Dansgaard-Oeschger oscillations. In a coupled climate model simulation which has accurately reproduced this oscillatory behavior for the first time, we show that formation of a glacial North Atlantic super polynya characterizes the initial stage of transition from cold stadial to warm interstadial conditions. The winter polynya forms within the otherwise sea ice-covered North Atlantic as a consequence of the onset of a thermohaline convective instability beneath an extensive stadial sea ice lid. Early in the stadial period, the tendency for thermal convective instability of an extensive warm pool beneath the sea ice lid is strongly inhibited by a stabilizing vertical salinity gradient, which gradually diminishes until a thermohaline convective instability occurs that leads to polynya formation and the rapid retreat of North Atlantic sea ice cover.

1. Introduction

Marine Isotopic Stage 3 (MIS3; approximately 60,000 to 30,000 years ago) was a period characterized by intense climate instability in the form of millennium timescale Dansgaard-Oeschger (D-O) oscillations [*Dansgaard et al.*, 1993]. Individual D-O oscillations are characterized by abrupt Northern Hemisphere warming events followed by gradual cooling periods and the temperature records inferred from Greenland δ^{18}O records [*Huber et al.*, 2006] are closely correlated with North Atlantic Ocean temperature [*Bond et al.*, 1997]. During MIS3, the occurrence of a warm Atlantic species group of foraminifera and depleted benthic δ^{18}O in marine sediment cores from the Norwegian Sea have been interpreted as pointing to an unstable vertical temperature gradient with a warm high-salinity Atlantic water mass below cold low-salinity polar surface water [*Rasmussen et al.*, 1996a, 1996b; *Rasmussen and Thomsen*, 2004; *Dokken et al.*, 2013].

Previous qualitative proposals intended to enhance understanding of the abrupt D-O warming phase have invoked a renewal of North Atlantic Deep Water (NADW) production associated with the disruption of a polar halocline, possibly associated with reduced glacial meltwater and iceberg discharge into the ocean [*Broecker et al.*, 1990; *Bond et al.*, 1992; *Sakai and Peltier*, 1997, 1999]. *Rasmussen and Thomsen* [2004] suggested on the contrary that subsurface warming gradually decreased the density of the intermediate depth water so as to lead to the onset of a thermal convective instability, which was imagined to destroy the polar halocline. Our model-based analyses, the first to reproduce this physical phenomenon and all of its primary characteristics [*Peltier and Vettoretti*, 2014, hereinafter PV14], have established not only that the D-O oscillation is expected only under generally cold glacial conditions but that its existence does not rely upon freshwater forcing of the North Atlantic Ocean to disrupt the overturning circulation. Furthermore, the model has also been shown to accurately explain the bipolar seesaw aspect of the D-O phenomenon through which the amplitude and phase relationships between the δ^{18}O signals in Greenland and Antarctic ice cores are established [*Vettoretti and Peltier*, 2015; PV14].

As we will show in what follows, the physical mechanism that underlies stadial-interstadial transitions in our model involves the onset of a thermohaline convective instability that develops beneath the extensive North Atlantic stadial sea ice cover through the erosion of the stabilizing effect of the halocline salinity gradient. The hallmark of the eventual instability that marks the onset of interstadial conditions is the formation of a "glacial super polynya" well north of the southern boundary of the sea ice lid.

2. Methods and Model

There are a number of plausible thermohaline convective instability-related processes that may be associated with a water column in which cold low-salinity water lies above warm high-salinity water. A simple convective instability associated with the double-diffusion process may occur in the polar halocline regime and be a viable mechanism for halocline destabilization [*Baines and Gill*, 1969]. Alternatively, a quadratic temperature term in a series expansion of the nonlinear equation of state (NEOS) of seawater gives rise to a diabatic phenomenon (cabbeling) that occurs when two parcels of water that are of the same density but of different temperature and salinity are combined along neutral density surfaces to produce a water mass that is of greater density than the original two parcels [*Foster*, 1972; *McDougall*, 1987; *Schanze and Schmitt*, 2013]. Similarly, the influence of thermobaricity [*Gill*, 1973; *McDougall*, 1984; *McDougall*, 1987] which depends upon the pressure dependence of the coefficient of thermal expansion of seawater is in principle also capable of leading to polar halocline instability. *Adkins et al.* [2005] and *Adkins* [2013] have suggested that such thermobaric instability could underlie the stadial interstadial transitions of interest to us here, but they invoked the possible importance of geothermal heat flux as a key ingredient needed to destabilize the water column.

We are employing the $1 \times 1°$ resolution Community Climate System Model Version 4 (CCSM4) [*Gent et al.*, 2011] to study the details of the D-O oscillation phenomenon. The condition for instability within the vertical mixing scheme of the approximately Boussinesq hydrostatic model of the ocean is solely dependent on the local Brunt-Väisälä frequency (N^2) of the water column. We are therefore limited in our ability to determine the relative importance of the subtle instability mechanisms described above. Nevertheless, the NEOS is of first-order importance since it determines the Brunt-Väisälä frequency which controls convective adjustment, the rate of exchange between the atmosphere and ocean, and the state of the global ocean stratification [*Roquet et al.*, 2015; *Nycander et al.*, 2015].

The simulation of modern Southern Ocean sea ice cover has been demonstrated to be sensitive to the vertical mixing scheme employed within an ocean model [e.g., *Losch et al.*, 2006; *Kjellsson et al.*, 2015]. The K-profile parameterization (KPP) [*Large et al.*, 1994] has previously been demonstrated to produce unphysical polynyas in the Southern Ocean in a coupled ocean-sea ice sectoral model of the Weddell Sea region [*Timmermann and Beckmann*, 2004]. The KPP parameterization is employed in the Parallel Ocean Program Version 2 (POP2) ocean component of CCSM4 that is implemented in the current study, but the control simulation does not exhibit such behavior. Polynya formation may also be sensitive to sea ice model parameterizations, but ocean and sea ice sensitivity studies will not be a focus of the current paper.

In contrast to the constant diapycnal diffusivity (κ) background profile employed for discussions in the main text of PV14, here we will present results for the D-O oscillation when the constant ($\kappa = 0.16$ cm^2/s) profile is replaced by the κ profile employed in the previous CCSM3 version of the model (e.g., see *Jayne* [2009] and supporting information). This κ profile captures the increase of diapycnal diffusivity below the main thermocline (to $\kappa = 1.0$ cm^2/s) that has been argued to be required in order to enable the deep water that forms at the poles to upwell to the surface in the Southern Ocean [e.g., *Munk*, 1966]. The ice age boundary conditions are provided by the ICE-6G_C (VM5a) model for paleotopography, bathymetry, and land ice cover [*Argus et al.*, 2014; *Peltier et al.*, 2015]. The boundary and initial conditions for the glacial and preindustrial simulations employed in this study have been discussed in detail in *Vettoretti and Peltier* [2013] and PV14.

3. Analyses

3.1. Statistical Equilibrium

The Atlantic Meridional Overturning Circulation (AMOC) strength under preindustrial (PI) boundary conditions is approximately 20 sverdrup (Sv, 10^6 m^3/s), when the same κ profile is employed as in the glacial experiment. This PI run has been spun off the PI control run from PV14 and run for an additional 1000 years, leading to no change in AMOC compared with PV14. The glacial simulation of 4500 calendar years was branched off the initial PV14 glacial experiment at year 1700 and was determined to have reached statistical equilibrium at year 2500. The glacial decadal average AMOC oscillates between a minimum stadial value of 8 Sv and a maximum interstadial value of 33 Sv (Figure 1a), which is somewhat larger than the peak-to-peak amplitude variations of the D-O oscillation described in the main text of PV14. Changes of 5°C in annual mean North Greenland Ice Core Project (NGRIP) surface temperature have previously been modeled with sensitivity experiments of low and high
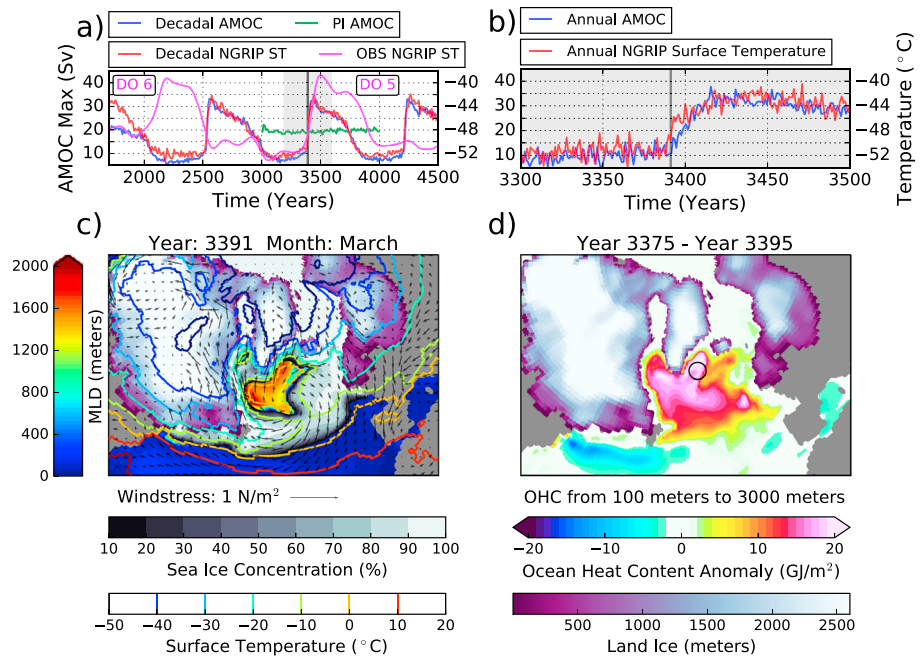
Figure 1. (a) Decadally averaged model preindustrial (green) and glacial (blue) AMOC and model NGRIP surface temperature (red). Observed NGIP temperature for D-O events 6 and 5 between 34,000 and 31,000 years before present (magenta) [*Huber et al.*, 2006]. (b) Annually averaged AMOC and NGRIP surface temperature in the area of the second D-O transition in the simulation (grey). (c) The polynya is demarcated by sea ice concentration < 10% and deep mixed layer depths (MLD). Atmospheric surface temperature and wind stress are also displayed. (d) The ocean heat content (OHC) anomaly 15 years before −5 years after the transition is calculated between 100 m and 3000 m in the model. Ice sheet topographic elevation is also displayed in Figures 1c and 1d.

sea ice cover in a climate model simulation of the Last Glacial Maximum over the North Atlantic [*Li et al.*, 2010]. The decadal average surface temperatures at NGRIP in our simulation (Figure 1a) increases to 10°C between the AMOC minimum and AMOC maximum and corresponds much more accurately with NGRIP-inferred surface temperature variability (Figure 1a) [*Huber et al.*, 2006]. The annually averaged NGRIP surface temperature and AMOC strength (Figure 1b) suggest that the temperature change at summit Greenland leads the AMOC transition somewhat, which implies a release of heat from a local sensible heat reservoir rather than heating associated with AMOC intensified meridional North Atlantic heat transport. The second D-O transition will be the focus of the following analyses, but it must be recognized that every stadial to interstadial transition in the simulation has the same characteristics (supporting information Figures S3–S5).

3.2. Glacial North Atlantic Super Polynyas

Polar sea ice-covered regions can develop open ocean areas called polynyas which are completely enclosed by sea ice or open areas that are partially flanked by land masses as well as sea ice. Latent heat polynyas are mechanically maintained by winds and ocean currents with newly formed sea ice being advected away from the formation regions. Thermally driven sensible heat polynyas often appear as a result of warm subsurface waters advected into the sea ice-covered region with the potential to melt the overlying sea ice cover [*Maqueda Morales et al.*, 2004]. *McPhee* [2003] was apparently the first to infer a climatic connection between D-O cycles and open ocean polynyas with thermobarically assisted convection, but involved arguments related to Southern Ocean processes. Recently, *Singh et al.* [2014] employed a simple heuristic column model of MIS3 Nordic Sea conditions and found that a parameterization of latent heat polynyas in their model was critical in their development of a heuristic understanding of the D-O oscillation. The super polynya that marks the onset of transition to stadial conditions in our model is, however, a sensible heat polynya as we discuss in what follows.

During the start of the warming phase of each of the simulated D-O cycles, the initial instability is coincident with the winter appearance of a large open ocean area measuring more than 10^6 km^2 that is entirely surrounded by sea ice (Figure 1c). This is approximately 3 times the area of the massive modern-day Weddell Sea polynya through the period from 1974 to 1976 [*Carsey*, 1980; *Martinson et al.*, 1981; *Gordon*, 1982; *Cheon et al.*, 2015]. In

this simulation, deep water formation is able to penetrate to depths between 1500 and 2000 m during winter in the polynya region while the North Atlantic region to the south remains sea ice covered. During the formation of this wintertime super polynya, the lower atmosphere over the North Atlantic is characterized by a strongly anticyclonic circulation which effects a wind stress mechanical forcing that tends to force sea ice inward toward the opening. The south to north wind flow over the polynya also provides a transport pathway for ocean sensible heat release to summit Greenland during the winter season.

The growth of the Northern Hemisphere continental ice sheets lowers sea level by approximately 120 m [*Peltier and Fairbanks*, 2006] thereby creating a stronger barrier to north-south transport at the location of the Denmark and Faroe Islands channels. Therefore, the cyclonic motion of the North Atlantic and Irminger Current deposits more sensible heat into the North Atlantic subpolar gyre. Furthermore, under glacial conditions the average global ocean salinity is increased by 1 practical salinity unit (psu) due to freshwater accumulated primarily in the Laurentide and Fennoscandian ice sheets (Figure 1d). Glacial intermediate waters are therefore more saline and result in an increase in polar halocline stratification and help to stabilize a strong thermocline temperature inversion. The ocean temperature reaches upward of 4–6°C just below the mixed layer and down to 1000 m depth just as has been inferred from benthic δ^{18}O records [*Dokken et al.*, 2013]. The ocean heat content (OHC) anomaly spanning a 20 year period across the D-O transition between 100 and 3000 m is upward of 20 GJ/m^2 in the polynya region (Figure 1d). *McPhee* [2003], in calculating the integrated sensible heat change from 1976 to 1997 in the Weddell Polynya from 150 m to 3000 m, found it to be approximately 4.6 GJ/m^2. Considering that 0.3 GJ/m^2 of latent heat energy is required to melt 1 m^3 of sea ice, we can assume that this heat reservoir can potentially melt the entire sea ice cover in the glacial North Atlantic and do so rapidly. This OHC anomaly is therefore an entirely suitable Available Potential Energy (APE) reservoir for the triggering of stadial-interstadial transitions.

3.3. Glacial Polynya Water Mass Structure

The water mass properties of the polynya region in Figure 1c are used to produce March temperature-salinity (*T-S*) diagrams immediately before (year 3389) and after (year 3392) the D-O warming transition (Figures 2a and 2b). The *T-S* diagram employs a very simplified three-term equation of state in potential density anomaly referenced to the surface (σ_0), which describes to a very high degree of accuracy the density in the polar halocline region, namely, $\sigma_0 = \beta S + \alpha T + \gamma T^2$, where $\beta = 0.8031$, $\alpha = -0.0554$, and $\gamma = -0.0065$ (see supporting information). The fidelity of the match with an 80-term expansion of the NEOS for σ_0 demonstrates excellent agreement [*Fofonoff and Millard*, 1983]. A *T-S* diagram of a well-defined polar halocline has the characteristic feature displayed in Figure 2a with much of the stadial surface and intermediate water masses spanning the 28.5σ_0 surface. After the transition, a rapid thermohaline convective instability in the entire polynya region mixes the water mass, thereby destroying the halocline and producing a more uniformly mixed water mass as there is a clear intersection of the surface, intermediate, and deeper water masses (Figure 2b).

The vertical profiles of horizontally averaged temperature and salinity before and after the D-O transition (Figure 2c) demonstrate that the average stadial warm pool temperature below the strong near-surface pycnocline is approximately 1.5°C. The stadial is characterized by both a strong thermocline and strong halo-cline at 100 m depth, with the stable salinity profile dominating the stratification at these low temperatures. After the transition the polynya becomes well mixed and almost unstratified from the surface to 2000 m depth (see also supporting information Figure S6). The relative contributions of temperature and salinity to the densification of the vertical density profile through the transition are quantified by displaying the density changes associated with each of the three terms in the approximate NEOS (Figure 2d). The change in salinity through the transition event has the tendency to reduce the density in the vertical while the loss of heat to the atmosphere tends to increase the density of the vertical profile. The temperature dominates the density increase from 100 to 1500 m while increases in salinity dominate the increases in the mixed layer after the transition. The cabbeling term indicates that this nonlinear temperature term accounts for 20% of the density increase from the base of the mixed layer to 1000 m depth on average. It is interesting to note that the polynya center of mass (CM) in the top 2200 m drops from 1100 m before to 1750 m after the transition and that the average thermosteric drop in sea level in the polynya region is approximately 3 m across the transition.

The mixing of water mass through the region of the sharp pycnocline would result in buoyancy loss and dianeutral mixing due to cabbeling. Here we diagnose the approximate increase in density that can potentially
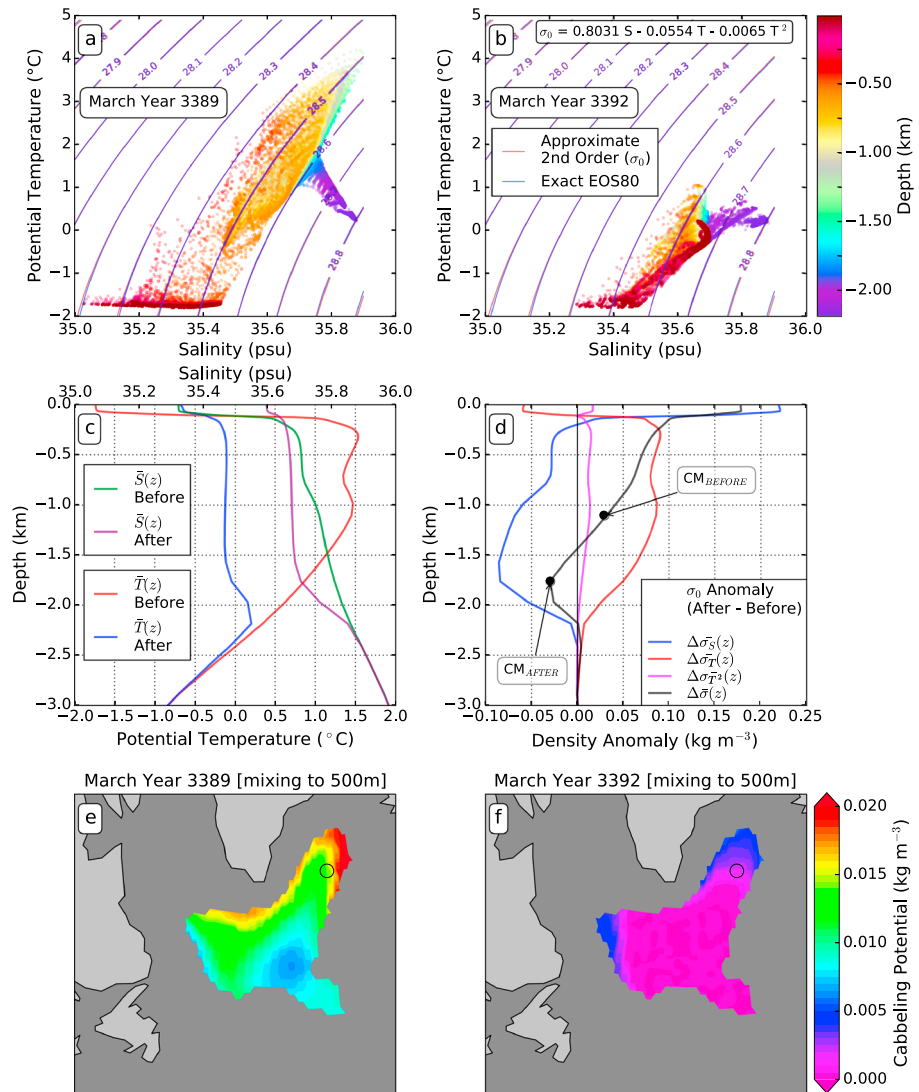
Figure 2. (a and b) The three-term expansion (red contours) of the NEOS is compared with the EOS80 solution (blue contours). The temperature-salinity diagram for the volume of polynya water demarcated in Figure 1c is shown (Figure 2a) 2 years before and (Figure 2b) 1 year after the polynya formation. (c) The vertical profile of temperature and salinity horizontally averaged over the polynya region before and after the transition. (d) The vertical profile of the density changes through the transition in the polynya region due to S (blue), T (red), T^2 (magenta), and the total change (black). CM = center of mass of the top 2200 m of water column. The potential increase in density due to cabbeling in the top 500 meters (e) before and (f) after the transition.

occur due to complete mixing in the polynya before and after the transition, in terms of what we define as cabbeling potential (see supporting information). In Figures 2e and 2f, the cabbeling potential associated with the complete vertical mixing in the top 500 m of the water column is plotted over the polynya formation region. The largest increase in density due to cabbeling occurs in the northern area of the polynya where the thermocline gradient is largest and where the initial instability occurs. The magnitude of the density increase due to cabbeling in our model also agrees with typical density increases due to cabbeling calculated from observations in the Greenland Basin [*Kasajima and Johannessen*, 2009]. Therefore, cabbeling could play an important role in the strength of the convective event through increases in dianeutral velocities resulting from density increases upon mixing [*Harcourt*, 2005].

3.4. Thermohaline Instability in D-O Warming Events

In the coupled model, the column remains stable until the square of the Brunt-Väisälä frequency (N^2) in the model attains a negative value during an ocean time step. The model convective parameterization then
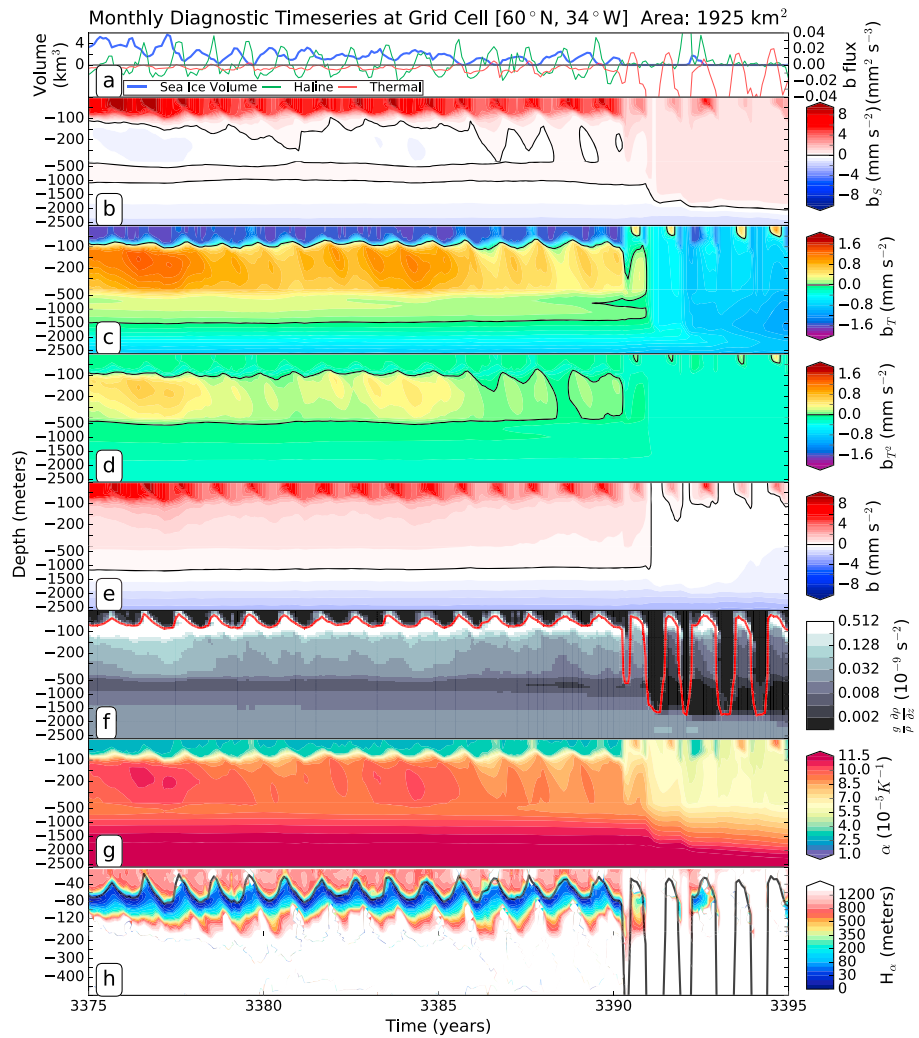
Figure 3. Time series of the vertical profile at the location of the initial instability indicated by the black circle in Figure 1d. (a) Ice volume (blue), thermal (red), and haline (green) surface buoyancy fluxes, (b) buoyancy due to the salinity term in the three-term NEOS (b_S), (c) buoyancy due to the linear temperature term (b_T), (d) buoyancy due to the quadratic temperature term ($b_T{}^2$), (e) total buoyancy (b), (f) buoyancy frequency (N^2), (g) thermal expansion coefficient (α), and (h) the thermobaric scale height (H_α). The mixed layer depth in the model is shown in Figures 3f and 3h with red and black contours, respectively.

increases the vertical turbulent diffusivities for heat and salt to very high values to remove the static instability [*Smith et al.*, 2010]. As this relatively coarse resolution model does not solve an explicit equation for vertical momentum, but rather employs the hydrostatic approximation, we are unable to describe the precise nature of this instability. Our intention in continuing work is to employ a nested nonhydrostatic model configuration to explicitly resolve the details of the mixing process.

In Figure 1d the black circle in the subpolar gyre highlights the location in which the convective instability first appears in the second D-O cycle. A number of time-dependent physical properties of the vertical water column are displayed in Figure 3. The sea ice volume gradually decreases until the area is seasonally ice free, coincident with the occurrence of the initial instability (Figure 3a). The surface buoyancy flux indicates that the haline component of the flux during winter (mainly due to sea ice formation) is larger than the thermal component (heat transfer to the atmosphere) before the transition (Figure 3a). The vertical buoyancy profile can be broken down into the contributions from temperature and salinity using our three-term NEOS. In the mixed layer and pycnocline, the halocline salinity gradient (Figure 3b) counteracts the propensity for cold water to sink in the mixed layer and warm pycnocline waters to rise from below. The decrease in buoyancy

in the winter mixed layer is associated with the gradual increase in salinity (Figure 3b). This is in spite of the melting of overlying sea ice from Figure 3a which acts to freshen the surface and increase buoyancy. There are of course horizontal transports of sea ice into and out of the area and salinity transports into the mixed layer both horizontally and from below. Overall, the balance is in favor of increasing mixed layer salinity. The buoyancy associated with both the linear and quadratic temperature terms in the NEOS (Figures 3c and 3d) is approximately 30% smaller in the mixed layer until the salinity increases to a critical value where the total buoyancy goes negative at the transition (Figure 3e).

The decrease in buoyancy in the subsurface warm pool (but not in the mixed layer) as the transition is approached is somewhat suggestive of the vertical diffusion of heat into the mixed layer and conversion of this heat into the latent heat required to melt sea ice (i.e., the mixed layer temperature is maintained at the freezing point as the sea ice decreases). The horizontally uniform model κ in the upper ocean (0.1 cm^2/s) is an order of magnitude greater than the turbulent κ observed in the modern Arctic Ocean polar halocline [*Zhang and Steele*, 2007; *Nguyen et al.*, 2009]. Also, the diffusive convection parameterization employed in the model is active in the sea ice-covered regions of this simulation in the base of the mixed layer. The parameterization adds to the prespecified column diapycnal diffusivity according to a criterion dependent upon a measure of the stability ratio, $\left(R_\rho = \alpha \frac{\partial T}{\partial z} / \beta \frac{\partial S}{\partial z}\right)$ in the diffusive convection regime such that $0 < R_\rho < 1$ and therefore acts to enhance the turbulent κ in this region (see supporting information Figures S7 and S8). These factors are likely important in the model simulation of polar haloclines and could play a role in the behavior of the D-O cycle.

The influence of the convective adjustment scheme in the model is best appreciated by plotting the model buoyancy frequency (N^2) on a logarithmic scale along with the mixed layer depth (Figure 3f). The highest values of N^2 at depths between 50 and 150 m are most stable to perturbation and are thus most stably stratified, preventing the release of subsurface heat to the atmosphere. This region is thinner in winter than in summer and is only penetrated by the mixed layer during the winter season right at the D-O warming transition. We conclude that the salinification of the winter mixed layer reaches a critical point as the surface ocean transitions to a state of nonperennial sea ice, which subsequently destabilizes the water column and initiates the formation of the glacial super polynya.

It has been hypothesized that thermobaric instability might be an important mechanism in the onset of deep water formation in the Greenland and Weddell Seas [*Akitomo*, 1999a, 1999b; *McPhee*, 2003; *Akitomo*, 2011]. A unique feature of this glacial stadial polar halocline is the rapid increase in the thermal expansion coefficient with depth ($\alpha(z)$) in this region of the North Atlantic. In fact, α increases by a factor of 3 as we transition through the pycnocline at 100 m depth (Figure 3g). In this region, the potential temperature and salinity then decrease from approximately 200 to 500 m, below a maximum which exists beneath the base of the mixed layer (see supporting information Figure S8). Scaling analysis has been used to investigate the propensity for thermobaric convection in polar regions using a measure of the vertical gradient of the thermal expansion coefficient [e.g., *Garwood et al.*, 1994; *Akitomo*, 1999a].

The increase in the density in sinking water with depth due to the thermobaric effect needs to exceed the background density gradient below the mixed layer in order for instability to occur. Our analyses (not shown) indicate that the mean conditions in this region are highly susceptible to thermobaric "plume" convection, referred to as Type-II convection [e.g., see *Akitomo*, 2011]. The thermobaric scale height ($H_\alpha = \alpha(z)/\partial \alpha/\partial z$) calculated at each model level is shown in Figure 3h. The surface value in this region has a scale height of 900 m and is typical of the value used in the previous scaling analyses. This scale height can be used to describe the loss in buoyancy of a cold parcel of seawater which is displaced vertically to a depth where the surrounding warmer water has potential temperature ($\delta\theta$). This loss of buoyancy influences the tendency of this parcel to return to its equilibrium position or to become vertically unstable. The loss of buoyancy or the reduction in N^2 can be expressed as $\frac{\delta b}{\delta z} = N^2 - \frac{g \, \alpha(z)}{H_\alpha} \delta\theta$ [see *Garwood et al.*, 1994; *Vallis*, 2006; *Nycander et al.*, 2015]. Many of the previous analyses do not consider the strong change in the vertical gradient of α near the base of the mixed layer in the polar halocline. This strong gradient implies that fluid parcels that are perturbed in the vertical, possibly associated with strong brine rejection during sea ice formation, would be highly susceptible to buoyancy loss near 100 m, a region where the stratification is most stable (Figure 3f). The influence of the thermobaric effect on the stability of the water column and instability associated with diffusive convection will be addressed in more detail elsewhere.

4. Conclusions

In this analysis we have presented a novel simulation demonstrating the role of the appearance of glacial super polynyas in the North Atlantic at the onset of D-O warming events. It is through the action of a thermohaline convective instability that occurs beneath the stadial North Atlantic sea ice lid that transition into the interstadial phase of the D-O oscillation is initiated. Once the polynya is opened by thermohaline convective instability, the large reservoir of sensible heat that is recharged during the stadial phase of the D-O cycle is released to the atmosphere and subsequently transported to summit Greenland and elsewhere. Although NADW production begins immediately with the onset of the thermohaline convective instability, the full interstadial AMOC strength is delayed by a few decades. These initial atmospheric temperature anomalies observed at summit Greenland are reinforced by the full reactivation of the AMOC. The increasing trend in the salinification of the winter mixed layer and the erosion of sea ice cover in the polar halocline due to upward turbulent diffusion of heat from below the mixed layer may be important mechanisms that trigger the D-O warming instability in this model. The surface salinity changes dominate the vertical buoyancy profile as a result of the first-order salinity contribution to the NEOS in this cold polar ocean environment. The use of a NEOS for seawater may prove to be a critical component for understanding the detailed nature of the thermohaline instability process that is synchronous with rapid D-O warming events.

References

Adkins, J. F. (2013), The role of deep ocean circulation in setting glacial climates, *Paleoceanography*, *28*, 539–561, doi:10.1002/palo.20046.

Adkins, J. F., A. P. Ingersoll, and C. Pasquero (2005), Rapid climate change and conditional instability of the glacial deep ocean from the thermobaric effect and geothermal heating, *Quat. Sci. Rev.*, *24*(5), 581–594.

Akitomo, K. (1999a), Open-ocean deep convection due to thermobaricity: 1. Scaling argument, *J. Geophys. Res.*, *104*, 5225–5234, doi:10.1029/1998JC900058.

Akitomo, K. (1999b), Open-ocean deep convection due to thermobaricity: 2. Numerical experiments, *J. Geophys. Res.*, *104*, 5235–5249, doi:10.1029/1998JC900062.

Akitomo, K. (2011), Two types of thermobaric deep convection possible in the Greenland Sea, *J. Geophys. Res.*, *116*, C08012, doi:10.1029/2010JC006635.

Argus, D. F., W. R. Peltier, R. Drummond, and S. Moore (2014), The Antarctic component of glacial isostatic adjustment model ICE-6G_C (VM5a) based upon GPS measurements of vertical motion of the crust, exposure age dating of ice thickness variations and relative sea level histories, *Geophys J. Int*, *198*(1), 537–563.

Baines, P. G., and A. E. Gill (1969), On thermohaline convection with linear gradients, *J. Fluid Mech.*, *37*(02), 289–306.

Bond, G., et al. (1992), Evidence for massive discharges of icebergs into the North Atlantic Ocean during the last glacial period, *Nature*, *360*, 245–249.

Bond, G., W. Showers, M. Cheseby, R. Lotti, P. Almasi, P. Priore, H. Cullen, I. Hajdas, and G. Bonani (1997), A pervasive millennial-scale cycle in North Atlantic Holocene and glacial climates, *Science*, *278*(5341), 1257–1266.

Broecker, W. S., G. Bond, M. Klas, G. Bonani, and W. Wolfli (1990), A salt oscillator in the glacial Atlantic? 1. The concept, *Paleoceanography*, *5*, 469–477, doi:10.1029/PA005i004p00469.

Carsey, F. D. (1980), Microwave observation of the Weddell Polynya, *Mon. Weather Rev.*, *108*(12), 2032–2044.

Cheon, W. G., S.-K. Lee, A. L. Gordon, Y. Liu, C.-B. Cho, and J. J. Park (2015), Replicating the 1970s' Weddell Polynya using a coupled ocean-sea ice model with reanalysis surface flux fields, *Geophys. Res. Lett.*, *42*, 5411–5418, doi:10.1002/2015GL064364.

Dansgaard, W., et al. (1993), Evidence for general instability of past climate from a 250-kyr ice-core record, *Nature*, *364*(6434), 218–220.

Dokken, T. M., K. H. Nisancioglu C. Li, D. S. Battisti, and C. Kissel (2013), Dansgaard-Oeschger cycles: Interactions between ocean and sea ice intrinsic to the Nordic seas, *Paleoceanography*, *28*, 491–502, doi:10.1002/palo.20042.

Fofonoff, N. P., and Millard Jr, R. C. (1983), Algorithms for computation of fundamental properties of seawater, Endorsed by Unesco/SCOR/ICES/IAPSO Joint Panel on Oceanographic Tables and Standards and SCOR Working Group 51. Unesco Tech. Pap. in Mar. Sci., No. 44.

Foster, T. D. (1972), An analysis of the cabbeling instability in sea water, *J. Phys. Oceanogr.*, *2*(3), 294–301.

Garwood, R. W., S. M. Isakari, and P. C. Gallacher (1994), Thermobaric convection, in *The Polar Oceans and Their Role in Shaping the Global Environment*, edited by O. M. Johannessen, R. D. Muench, and J. E. Overland, pp. 199–209, AGU, Washington, D. C.

Gent, P. R., et al. (2011), The community climate system model version 4, *J. Clim.*, *24*(19), 4973–4991.

Gill, A. E. (1973), Circulation and bottom water production in the Weddell Sea, *Deep Sea Res. Oceanogr. Abstr.*, *20*, 111–140.

Gordon, A. L. (1982), Weddell deep water variability, *J. Mar. Res.*, *40*(suppl), 199–217.

Harcourt, R. R. (2005), Thermobaric cabbeling over Maud Rise: Theory and large eddy simulation, *Prog. Oceanogr.*, *67*(1), 186–244.

Huber, C., M. Leuenberger, R. Spahni, J. Flückiger, J. Schwander, T. F. Stocker, JohnsenS. , A. Landais, and J. Jouzel (2006), Isotope calibrated Greenland temperature record over Marine Isotope Stage 3 and its relation to CH 4, *Earth Planet. Sci. Lett.*, *243*(3), 504–519.

Jayne, S. R. (2009), The impact of abyssal mixing parameterizations in an ocean general circulation model, *J. Phys. Oceanogr.*, *39*(7), 1756–1775.

Kasajima, Y., and T. Johannessen (2009), Role of cabbeling in water densification in the Greenland Basin, *Ocean Sci.*, *5*(3), 247–257.

Kjellsson, J., P. R. Holland, G. J. Marshall, P. Mathiot, Y. Aksenov, A. C. Coward, S. Bacon, A. P. Megann, and J. Ridley (2015), Model sensitivity of the Weddell and Ross seas, Antarctica, to vertical mixing and freshwater forcing, *Ocean Model.*, *94*, 141–152.

Large, W. G., J. C. McWilliams, and S. C. Doney (1994), Oceanic vertical mixing: A review and a model with a nonlocal boundary layer parameterization, *Rev. Geophys.*, *32*, 363–403, doi:10.1029/94RG01872.

Li, C., D. S. Battisti, and C. M. Bitz (2010), Can North Atlantic sea ice anomalies account for Dansgaard-Oeschger climate signals?*, *J. Clim.*, *23*(20), 5457–5475.

Losch, M., S. Herlufsen, and R. Timmermann (2006), Effects of heterogeneous surface boundary conditions on parameterized oceanic deep convection, *Ocean model.*, *13*(2), 156–165.

Maqueda Morales, M. A., A. J. Willmott, and N. R. Biggs (2004), Polynya dynamics: A review of observations and modeling, *Rev. Geophys.*, *42*, RG1004, doi:10.1029/2002RG000116.

Martinson, D. G., P. D. Killworth, and A. L. Gordon (1981), A convective model for the Weddell Polynya, *J. Phys. Oceanogr.*, *11*(4), 466–488.

McDougall, T. J. (1984), The relative roles of diapycnal and isopycnal mixing on subsurface water mass conversion, *J. Phys. Oceanogr.*, *14*(10), 1577–1589.

McDougall, T. J. (1987), Thermobaricity, cabbeling, and water-mass conversion, *J. Geophys. Res.*, *92*, 5448–5464, doi:10.1029/JC092iC05p05448.

McPhee, M. G. (2003), Is thermobaricity a major factor in Southern Ocean ventilation?, *Antarct. Sci.*, *15*(01), 153–160.

Munk, W. H. (1966), Abyssal recipes, *Deep Sea Res. Oceanogr. Abstr.*, *13*, 707–730.

Nguyen, A. T., D. Menemenlis, and R. Kwok (2009), Improved modeling of the Arctic halocline with a subgrid-scale brine rejection parameterization, *J. Geophys. Res.*, *114*, C11014, doi:10.1029/2008JC005121.

Nycander, J., M. Hieronymus, and F. Roquet (2015), The nonlinear equation of state of sea water and the global water mass distribution, *Geophys. Res. Lett.*, *42*, 7714–7721, doi:10.1002/2015GL065525.

Peltier, W. R., D. F. Argus, and R. Drummond (2015), Space geodesy constrains ice age terminal deglaciation: The global ICE-6G_C (VM5a) model, *J. Geophys. Res. Solid Earth*, *120*, 450–487, doi:10.1002/2014JB011176.

Peltier, W. R., and R. G. Fairbanks (2006), Global glacial ice volume and Last Glacial Maximum duration from an extended Barbados sea level record, *Quat. Sci. Rev.*, *25*(23), 3322–3337.

Peltier, W. R., and G. Vettoretti (2014), Dansgaard-Oeschger oscillations predicted in a comprehensive model of glacial climate: A "kicked" salt oscillator in the Atlantic, *Geophys. Res. Lett.*, *41*, 7306–7313, doi:10.1002/2014GL061413.

Rasmussen, T. L., and E. Thomsen (2004), The role of the North Atlantic Drift in the millennial timescale glacial climate fluctuations, *Palaeogeogr. Palaeoclimatol. Palaeoecol.*, *210*(1), 101–116.

Rasmussen, T. L., E. Thomsen, L. Labeyrie, and T. C. van Weering (1996a), Circulation changes in the Faeroe-Shetland Channel correlating with cold events during the last glacial period (58–10 ka), *Geology*, *24*(10), 937–940.

Rasmussen, T. L., E. Thomsen, T. C. Weering, and L. Labeyrie (1996b), Rapid changes in surface and deep water conditions at the Faeroe Margin during the last 58,000 years, *Paleoceanography*, *11*, 757–771, doi:10.1029/96PA02618.

Roquet, F., G. Madec, L. Brodeau, and J. Nycander (2015), Defining a simplified yet realistic equation of state for seawater, *J. Phys. Oceanogr.*, *45*(10), 2564–2579.

Sakai, K., and W. R. Peltier (1997), Dansgaard-Oeschger oscillations in a coupled atmosphere-ocean climate model, *J. Clim.*, *10*(5), 949–970.

Sakai, K., and W. R. Peltier (1999), A dynamical systems model of the Dansgaard-Oeschger oscillation and the origin of the Bond cycle, *J. Clim.*, *12*(8), 2238–2255.

Schanze, J. J., and R. W. Schmitt (2013), Estimates of cabbeling in the global ocean, *J. Phys. Oceanogr.*, *43*(4), 698–705.

Singh, H. A., D. S. Battisti, and C. M. Bitz (2014), A heuristic model of Dansgaard–Oeschger cycles. Part I: Description, results, and sensitivity studies, *J. Clim.*, *27*(12), 4337–4358.

Smith, R., et al. (2010), The Parallel Ocean Program (POP) reference manual ocean component of the Community Climate System Model (CCSM) and Community Earth System Model (CESM), *Rep. LAUR-01853*, *141*.

Timmermann, R., and A. Beckmann (2004), Parameterization of vertical mixing in the Weddell Sea, *Ocean Model.*, *6*(1), 83–100.

Vallis, G. K. (2006), *Atmospheric and Oceanic Fluid Dynamics: Fundamentals and Large-Scale Circulation*, 745 pp., Cambridge Univ. Press, Cambridge, U. K.

Vettoretti, G., and W. R. Peltier (2013), Last Glacial Maximum ice sheet impacts on North Atlantic climate variability: The importance of the sea ice lid, *Geophys. Res. Lett.*, *40*, 6378–6383, doi:10.1002/2013GL058486.

Vettoretti, G., and W. R. Peltier (2015), Interhemispheric air temperature phase relationships in the nonlinear Dansgaard-Oeschger oscillation, *Geophys. Res. Lett.*, *42*, 1180–1189, doi:10.1002/2014GL062898.

Zhang, J., and M. Steele (2007), Effect of vertical mixing on the Atlantic Water layer circulation in the Arctic Ocean, *J. Geophys. Res.*, *112*, C04S04, doi:10.1029/2006JC003732.